AIAA JOURNAL
Vol. 36, No. 11, November 1998

Large-Eddy Simulation of a Spatially Evolving Supersonic Turbulent Boundary-Layer Flow

Evangelos T. Spyropoulos* and Gregory A. Blaisdell†
Purdue University, West Lafayette, Indiana 47907

Several issues involving the large-eddy simulation of wall-bounded compressible turbulent flows are investigated. A spatially evolving supersonic boundary layer is simulated using a high-order-accurate finite difference scheme and the dynamic subgrid-scale model. A parametric study suggests that the finite difference scheme has a detrimental effect on the resolution of the smaller scales due to excessive numerical dissipation from the spatial differencing. Also, because the dynamic model uses the smaller resolved-scale eddies to determine the model coefficients, the predicted coefficients do not have the appropriate values. The use of higher-order schemes is found to better capture the smaller resolved scales and to improve substantially the quality of the results. The effect of descretization errors on large-eddy simulation needs to be addressed further before proceeding with large-eddy simulation of flows of engineering interest.

I. Introduction

A SIGNIFICANT number of boundary-layer flow experiments have been performed that have greatly improved our knowledge of the effects of compressibility on turbulence. In addition, a number of catalogs and reviews of experimental data have been done, such as those by Fernholtz and Finley,[1,2] Fernholtz et al.,[3] Settles and Johnson,[4] Spina et al.,[5] Bradshaw,[6] and Lele.[7] Measuring turbulent quantities in this type of flow, however, is difficult.[8] Apart from being subject to considerable error, measurements are restricted away from the near-wall region.[9,10] On the other hand, due to computer limitations very little work has been accomplished numerically in complementing the experiments. The spatially developing case has been examined recently with direct numerical simulation (DNS) by Rai et al.,[11] and the temporal case by Childs and Reisenthel,[12] Hatay and Biringen,[13] and Guo and Adams.[14]

Also, in the past few years, there has been a resurgence of interest in performing large-eddy simulations (LES) of flows of engineering interest. There are two roles for LES to play in the computation of complex turbulent flows. First, LES can be used to study the physics of turbulence at higher Reynolds numbers than can currently be achieved with DNS, and LES can aid in the testing and improvement of lower-order engineering turbulence models. Second, it is hoped that LES can be used in the near future as an engineering tool rather than as a research tool. Although it will remain an expensive tool, it might be the only means of accurately computing complex flows for which lower-order models fail.

The majority of LES reported in the literature involve incompressible fluid flows that are homogeneous in at least two spatial directions. Although computation of such flows has greatly contributed to the development of LES, the computation of more complex flows is required. In this paper, the method is applied to a spatially developing, supersonic, flat-plate boundary-layer flow. The performance of the LES is evaluated based mainly on the DNS database of Rai et al.[11] Experimental data[1,15–17] are also used for comparison. A parametric study is performed to evaluate the dynamic subgrid-scale (SGS) model. In addition, several issues related to the effect of the numerical scheme on the simulations are investigated.

Received Oct. 28, 1996; presented as Paper 97-0429 at the AIAA 35th Aerospace Sciences Meeting, Reno, NV, Jan. 6–9, 1997; revision received May 27, 1998; accepted for publication June 11, 1998.

*Graduate Assistant, School of Aeronautics and Astronautics; currently Development Engineer, Centric Engineering Systems, Inc., Sunnyvale, CA 94086. Member AIAA.

†Associate Professor, School of Aeronautics and Astronautics. Senior Member AIAA.

II. Mathematical Formulation

A. Governing Equations

In LES one computes explicitly only the motion of the large-scale structures. The nonlinear interactions with the small scales are not captured and are modeled. The governing equations for the large eddies in compressible flows are obtained after filtering the continuity, momentum, and energy equations and recasting in terms of Favre averages. The filtering operation (denoted by an overbar) maintains only the large scales and can be written in terms of a convolution integral:

$$\bar{f}(x_1, x_2, x_3) = \int_D \prod_{i=1}^{3} G_i(x_i - x_i') f(x_1', x_2', x_3')\, \mathrm{d}x_1'\, \mathrm{d}x_2'\, \mathrm{d}x_3' \quad (1)$$

where f is a turbulent field, G_i is some spatial filter that operates in the ith direction and has a filter width Δ_i (usually equal to the computational grid spacing in that direction), and D is the flow domain.

The resulting equations of motion for the large eddies are as follows:

$$\frac{\partial \bar{\rho}}{\partial t} + \frac{\partial(\bar{\rho}\tilde{u}_i)}{\partial x_i} = 0 \quad (2)$$

$$\frac{\partial(\bar{\rho}\tilde{u}_i)}{\partial t} + \frac{\partial(\bar{\rho}\tilde{u}_i\tilde{u}_j)}{\partial x_j} = -\frac{\partial \bar{p}}{\partial x_i} + \frac{\partial}{\partial x_j}(\sigma_{ij} - \tau_{ij}) \quad (3)$$

$$\frac{\partial \bar{p}}{\partial t} + \frac{\partial(\bar{p}\tilde{u}_i)}{\partial x_i} = (\gamma - 1)\left[-\bar{p}\frac{\partial \tilde{u}_i}{\partial x_i} + \sigma_{ij}\frac{\partial \tilde{u}_j}{\partial x_i} + \frac{\partial}{\partial x_i}\left(\tilde{k}\frac{\partial \tilde{T}}{\partial x_i} - C_v q_i\right)\right] \quad (4)$$

where

$$\sigma_{ij} = \tilde{\mu}\left(\frac{\partial \tilde{u}_i}{\partial x_j} + \frac{\partial \tilde{u}_j}{\partial x_i} - \frac{2}{3}\frac{\partial \tilde{u}_k}{\partial x_k}\delta_{ij}\right) \quad (5)$$

The effects of the small scales are present in the preceding equations through the SGS stress tensor and the SGS heat flux, respectively,

$$\tau_{ij} = \bar{\rho}(\widetilde{u_i u_j} - \tilde{u}_i\tilde{u}_j), \qquad q_i = \bar{\rho}(\widetilde{u_i T} - \tilde{u}_i\tilde{T}) \quad (6)$$

and require modeling. A tilde is used to denote Favre averages ($\tilde{f} = \overline{\rho f}/\bar{\rho}$). Also, ρ is the density, T is the temperature, u_i is the velocity component in the i direction, and k is the thermal conductivity. The specific heats at constant volume C_v and at constant

pressure C_p are assumed in this study to be constant. The large-scale molecular viscosity $\tilde{\mu}$ is assumed to obey Sutherland's law:

$$\frac{\tilde{\mu}}{\tilde{\mu}_0} = \left(\frac{\tilde{T}}{\tilde{T}_0}\right)^{\frac{3}{2}} \frac{\tilde{T}_0 + \tilde{T}_e}{\tilde{T} + \tilde{T}_e} \tag{7}$$

with a Sutherland constant $\tilde{T}_e = 198.6°\text{R}$. The large-scale pressure $\bar{p}$ is obtained from the filtered equation of state, $\bar{p} = \bar{\rho} R \tilde{T}$. The molecular Prandtl number Pr is assumed to be 0.718. Note that in deriving Eqs. (2–4) the viscous, pressure-dilatation, and conduction terms were approximated in a similar fashion as by Erlebacher et al.[18] Based on these approximations, terms like the SGS viscosity fluctuations are neglected. Moin et al.[19] measured such terms for the case of compressible isotropic turbulence and found that they are negligible also. In the channel flow DNS examined in Ref. 20, the largest corresponding additional dissipation term in the context of Reynolds-averaged Navier–Stokes computation has a magnitude on the order of 6% for a Mach 1.5 case and 16% for a Mach 3 case. In an LES one would expect the magnitude of the corresponding SGS terms to be much less because the contribution of the resolved scales is included as part of the LES calculation.

B. Subgrid-Scale Modeling

The dynamic SGS modeling concept was introduced by Germano et al.[21] for LES of incompressible flows and has attracted a lot of attention in the LES community in recent years. Moin et al.[19] extented the dynamic model to compressible flows, and Lilly[22] suggested a refinement to both models that is now largely employed. Since then, further refinements to the model have been proposed.[23–25]

The model for the deviatoric and isotropic parts of the SGS stress tensor is based on Smagorinsky's[26] and Yoshizawa's[27] eddy-viscosity models, respectively. The model constants, however, are allowed to vary in space and time and are computed dynamically, as the simulation progresses, from the energy content of the smallest of the resolved large scales. This approach of calculating the model constants has been found to substantially improve the accuracy and robustness of the LES method because the model constants adjust dynamically to the local structure of the flow and do not have to be specified a priori. In addition, it has been found from incompressible flow simulations that the dynamic model provides the correct limiting behavior near solid boundaries and adjusts properly by itself in the transitional or laminar regimes. Although it cannot properly predict backscatter, it allows for some reverse energy cascade. A similar approach is followed for the SGS heat flux.

Dynamic modeling is accomplished with the aid of a second filter (referred to as the test filter $\hat{G}$) that has a filter width $\hat{\Delta}_i$ in the ith direction and that is coarser than the grid used to perform the computations ($\hat{\Delta}_i > \Delta_i$).

The model parameterization for the SGS stress and the SGS heat flux is given by

$$\tau_{ij} - \tfrac{1}{3}\tau_{kk}\delta_{ij} = -2\mu_t\left(\tilde{S}_{ij} - \tfrac{1}{3}\tilde{S}_{kk}\delta_{ij}\right) \tag{8}$$

$$\tau_{kk} = 2C_I\bar{\rho}\Delta^2\tilde{S}_M^2 \tag{9}$$

$$q_i = -\frac{\mu_t}{Pr_t}\frac{\partial\tilde{T}}{\partial x_i} \tag{10}$$

where $\mu_t = C\Delta^2\bar{\rho}\tilde{S}_M$, $\tilde{S}_{ij} = 0.5(\partial\tilde{u}_i/\partial x_j + \partial\tilde{u}_j/\partial x_i)$, $\tilde{S}_M = (2\tilde{S}_{ij}\tilde{S}_{ij})^{1/2}$, and $\Delta = (\Delta x\Delta y\Delta z)^{1/3}$.

The model coefficients are computed from

$$C = \frac{\left\langle\left(\mathcal{L}_{ij} - \tfrac{1}{3}\mathcal{L}_{kk}\delta_{ij}\right)M_{ij}\right\rangle}{\langle M_{pq}M_{pq}\rangle} \tag{11}$$

$$C_I = \frac{\langle\mathcal{L}_{kk}\rangle}{\left\langle 2\hat{\Delta}^2\hat{\bar{\rho}}|\hat{\tilde{S}}|^2 - 2\Delta^2\widehat{\bar{\rho}\tilde{S}_M^2}\right\rangle} \tag{12}$$

$$Pr_t = C\frac{\langle N_i N_i\rangle}{\langle -K_j N_j\rangle} \tag{13}$$

where $\hat{}$ denotes test-filtered quantities, $\hat{\Delta} = (\hat{\Delta}_1\hat{\Delta}_2\hat{\Delta}_3)^{1/3}$, $\langle\,\rangle$ denotes averaging over the homogeneous spanwise direction, and

$$\mathcal{L}_{ij} = \widehat{\bar{\rho}\tilde{u}_i\tilde{u}_j} - (1/\hat{\bar{\rho}})\widehat{\bar{\rho}\tilde{u}_i}\,\widehat{\bar{\rho}\tilde{u}_j} \tag{14}$$

$$M_{ij} = -2\hat{\Delta}^2\hat{\bar{\rho}}\hat{\tilde{S}}_M\left(\hat{\tilde{S}}_{ij} - \tfrac{1}{3}\hat{\tilde{S}}_{kk}\delta_{ij}\right) + 2\Delta^2\widehat{\bar{\rho}\tilde{S}_M\left(\tilde{S}_{ij} - \tfrac{1}{3}\tilde{S}_{kk}\delta_{ij}\right)} \tag{15}$$

$$N_i = \hat{\Delta}^2\hat{\bar{\rho}}\hat{\tilde{S}}_M\frac{\partial\hat{\tilde{T}}}{\partial x_i} - \Delta^2\widehat{\bar{\rho}\tilde{S}_M\frac{\partial\tilde{T}}{\partial x_i}} \tag{16}$$

$$K_i = \widehat{\bar{\rho}\tilde{u}_i\tilde{T}} - (1/\hat{\bar{\rho}})\widehat{\bar{\rho}\tilde{u}_i}\,\widehat{\bar{\rho}\tilde{T}} \tag{17}$$

In the simulations, negative values for the eddy viscosity μ_t were allowed as long as the total viscosity ($\mu_T = \tilde{\mu} + \mu_t$) and the total thermal conductivity ($k_T = \tilde{k} + C_v\mu_t/Pr_t$) were nonnegative. This restricts the amount of energy backscatter allowed but avoids numerical instabilities due to antidissipation. A three-point, top-hat filter (derived using the trapezoidal integration rule) was employed for the test filtering.

III. Numerical Method

The DNS code of Rai et al.[11] was modified to perform LES using the dynamic model. The DNS code solves the Navier–Stokes equations in nonconservative form. Because the problem considered here does not exhibit discontinuities, the same approach was taken in the LES to solve Eqs. (2–4). Flux splitting is employed on the inviscid (Euler) fluxes along each spatial direction to decompose them into signals that propagate on opposite characteristic lines.[28] Following Ref. 11, the spatial derivatives of the split fluxes are computed using fifth-order-accurate, upwind-biased finite differences. The viscous terms and the derivatives in the dynamic model are computed using fourth-order-accurate central differences. Time advancement is performed using an iterative fully implicit second-order-accurate scheme.[29] Such schemes are unconditionally stable and allow for accurate advancement using much larger time steps than explicit schemes. However, they are more CPU intensive because they involve the solution of a system of algebraic equations. In addition, upwind schemes are much more stable than central difference schemes because they provide implicitly some artificial dissipation. The latter also reduces aliasing errors by dissipating the energy content of the flowfield at higher resolved wave numbers. A discussion regarding the accuracy of the method in LES is presented in Sec. VI. Also, a truncation error analysis for such schemes is presented in Ref. 30.

IV. Reference Case

The case considered in the DNS of Rai et al.[11] and in the current LES is the zero-pressure-gradient, flat-plate boundary-layer flow experiment by Shutts et al.[15] with a freestream Mach number of 2.25 (this experiment is also discussed in Ref. 1; see case 55010501). The Reynolds number based on freestream conditions is 6.35×10^5/in. The adiabatic wall temperature is 580°R, and the temperature at the freestream is 305°R. Measurements were taken on the centerline of the plate at a streamwise location where the Reynolds number with respect to the momentum thickness, Re_θ, was 6.053×10^3. Mean flowfield data were obtained at 17 locations in the wall-normal direction using a pitot tube. Turbulence fluctuations data were not taken, and so only limited mean flow data are available for comparison to the simulations. In some other experiments, measurements of turbulence fluctuations are reported.[2,3,5] However, these experiments are at very high Reynolds or Mach numbers and cannot be simulated currently by DNS or LES. In addition, as was mentioned earlier, a wide variation in the value of the peak turbulence intensity is found in such data, which makes these measurements less reliable.

The computation of Rai et al.[11] is the first DNS of a compressible, turbulent, supersonic, spatially evolving boundary-layer flow. The flow conditions were chosen to match the conditions in the experiments of Shutts et al.[15] (see Ref. 1) for two reasons. First, the reported experimental data are at low freestream Re_θ and can

Table 1 Case parameters for the boundary-layer flow simulations

Case	Type	N_x (I, II, III)	N_y	N_z	$\mathcal{A}$, %	τ_{kk}	Test filter in
A1	LES, fourth order	416 (116, 281, 21)	55	257	4	Model	x, y, z
A2	DNS, fourth order	416 (116, 281, 21)	55	257	4	——	——
B1	LES, fourth order	416 (116, 281, 21)	55	129	4	Model	x, y, z
B2	LES, fourth order	416 (116, 281, 21)	55	129	6	Model	x, y, z
B3	LES, fourth order	416 (116, 281, 21)	55	129	6	Neglect	x, y, z
B4	LES, second order	416 (116, 281, 21)	55	129	4	Model	x, y, z
C1	LES, fourth order	311 (116, 176, 21)	55	65	4	Model	x, y, z
C2	LES, fourth order	311 (116, 176, 21)	55	65	4	Model	x, z
C3	LES, fourth order	311 (116, 176, 21)	55	65	10	Model	x, y, z
C4	LES, second order	311 (116, 176, 21)	55	65	4	Model	x, y, z
DNS	DNS,[11] fourth order	971 (231, 701, 41)	55	321	4	——	——

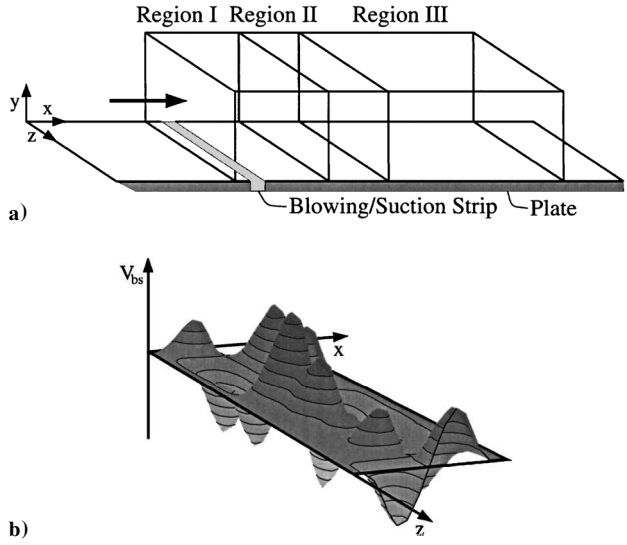

Fig. 1 a) Schematic of the computational domain and b) blowing and suction mechanism.

be computed using DNS. In fact, $Re_\theta = 6 \times 10^3$ is considered very high for a DNS but can be simulated because the molecular viscosity is higher closer to the wall, where the grid requirements are most stringent, because the temperature in this case is higher there and, therefore, a coarser grid can be used.[11] Second, the experiment is at supersonic, and not hypersonic, freestream conditions. At high Mach numbers ($M > 5$), the compressibility effects are very strong, and the numerical schemes currently available are not able to accurately simulate such flows.

V. Calculation Setup

The size of the computational domain (Fig. 1a) and the type of boundary conditions are chosen to be the same as in the DNS[11] for consistency. As is shown in Fig. 1, the domain contains a narrow strip on the wall located 0.5 in. from the inlet, through which disturbance waves are introduced to the flow by periodic blowing and suction. This type of tripping mechanism has been found by Konzelmann et al.[31] (see also Ref. 32) to generate waves without excessive acoustic contamination (pure vorticity waves). The computational domain is divided along the streamwise direction into three regions. The first region is 3 in. long and contains the regions of blowing and suction, as well as transition. The second region has uniform spacing in x, is 2 in. long, and contains the turbulent region. The third region is 6 in. long and becomes gradually very coarse to artificially dissipate all of the turbulent fluctuations. In this way, waves may be controlled so that they do not reflect back into the domain, when they reach the outlet boundary, and contaminate the turbulent fields in the other regions. A similar grid coarsening is applied outside the boundary layer in the wall-normal direction.[11] The domain is 0.35 in. wide in the span and 3 in. tall along the wall-normal direction. The discretization used in the various cases considered is discussed further later.

The no-slip boundary condition is imposed on the lower boundary (surface of plate), except at the region of blowing and suction ($4.5 \le x \le 5$), where the normal velocity component at the lower boundary is set to v_{bs}, which is as follows[11]:

$$v_{bs} = \mathcal{A} U_\infty f(x) g(z) h(t) \tag{18}$$

where

$$f(x) = 4 \sin\theta(1 - \cos\theta)/27^{\frac{1}{2}}, \qquad \theta = 2\pi(x - x_a)/(x_b - x_a)$$

$$g(z) = \sum_{l=0}^{l_{\max}} Z_l \sin[2\pi l(z/z_{\max} + \phi_l)]$$

$$\sum_{l=0}^{l_{\max}} Z_l = 1, \qquad Z_l = 1.25 Z_{l+1}$$

$$h(t) = \sum_{m=0}^{m_{\max}} T_m \sin[2\pi m(\beta t + \phi_m)]$$

$$\sum_{m=1}^{m_{\max}} T_m = 1, \qquad T_m = 1.25 T_{m+1}$$

and where $l_{\max} = 10$, $m_{\max} = 5$, $x_a = 4.5$ in., $x_b = 5$ in., $\mathcal{A}$ is the disturbance amplitude (see Table 1), $\beta = 75{,}000$ Hz, ϕ_l and ϕ_m are random numbers (between 0 and 1), and $z_{\max} = 0.35$ in. The blowing and suction mechanism is shown schematically in Fig. 1b. At the wall, the temperature is set to the adiabatic wall temperature T_{aw}, and the pressure is set the same as its value one grid point above the wall.

At the inflow boundary (inlet boundary of region I), the flow is fixed based on a laminar boundary-layer analysis. The incoming flow is supersonic everywhere except in the subsonic portion of the boundary layer, as is the flow at the outlet boundary of region III, as well. At the outflow boundary node points the dependent variables are set the same as their values at one grid point upstream of the exit location, with the exception of the pressure at subsonic locations, which is set to the pressure at the first grid point upstream of the exit location (on the same vertical grid line) that becomes supersonic.

At the spanwise boundaries, a periodic boundary condition is imposed because the flow is homogeneous along the span. Finally, the flow is assumed symmetric with respect to the upper boundary because this boundary is located well away from the edge of the boundary layer.

VI. Results

A. Case Definitions

A number of simulations were conducted to examine several issues regarding the accuracy of the LES method in computing spatially evolving supersonic boundary-layer flows using finite difference schemes. The cases considered are summarized in Table 1. They are categorized in three sets (A, B, and C), based on the grid resolution. The grid resolutions in terms of physical units and wall units (based on the friction velocity close to the end of the turbulent region, $x = 8.8$ in.) are given in Tables 2 and 3, respectively. The grid spacing is varied in the simulations along the streamwise direction in region II, which contains the turbulent field, and along the spanwise direction. The grid resolution in the x direction is kept the same in regions I and III for all cases. In addition, the same number of points is used in the wall-normal direction for all cases. The effect of the numerical scheme is examined in cases B1 and B4

Table 2 Grid resolution in physical units at $x = 8.8$ in.

Case	Δx, in.	$\Delta y_{\min}$, in.	Δz, in.
A1, A2	0.00714	0.0001	0.00137
B1–B4	0.00714	0.0001	0.00273
C1–C4	0.01143	0.0001	0.00547
DNS	0.00286	0.0001	0.00109

Table 3 Grid resolution in wall units at $x = 8.8$ in.

Case	Δx^+	$\Delta y^+_{\min}$	Δz^+
A1, A2	59.0	0.87	11.4
B1–B4	59.3	0.83	22.7
C1–C4	88.0	0.77	42.1
DNS	27.0	0.94	10.3

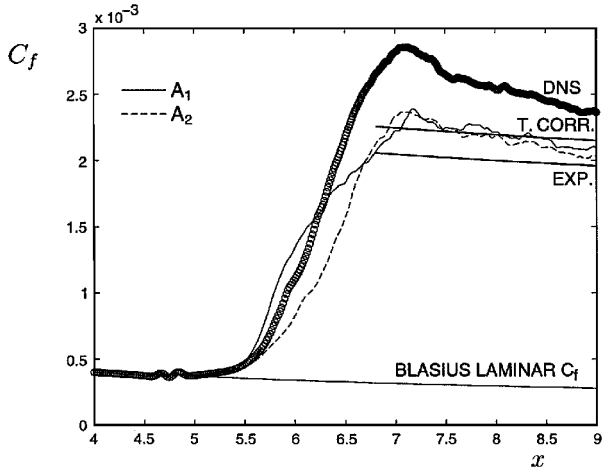

Fig. 2 Skin-friction coefficient for case set A.

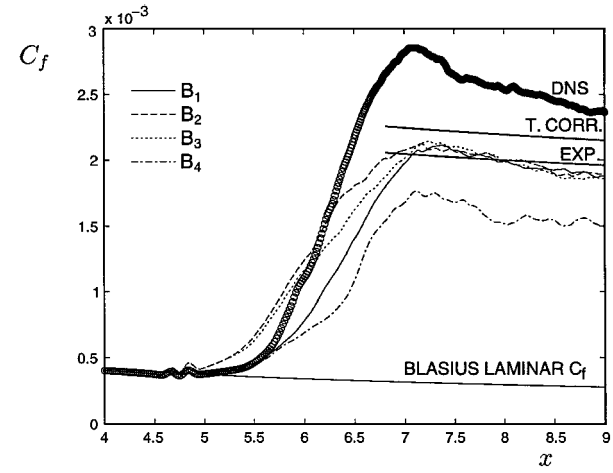

Fig. 3 Skin-friction coefficient for case set B.

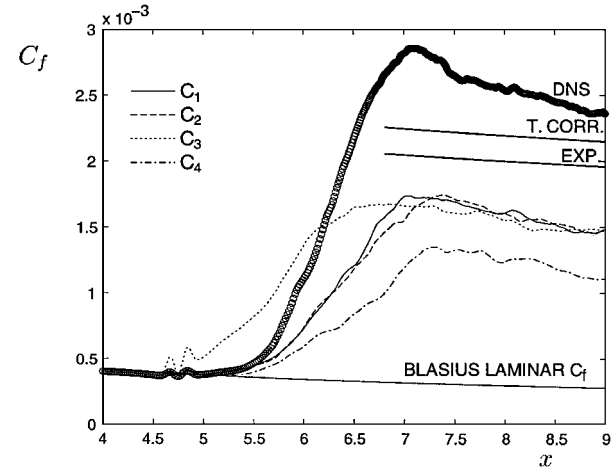

Fig. 4 Skin-friction coefficient for case set C.

and cases C1 and C4. The effect of the disturbance amplitude used in the blowing and suction on transition is examined in cases B1 and B2 and cases C1 and C3. The effect of not modeling the trace of the SGS stresses is examined in cases B2 and B3. The effect of not test (and grid) filtering in the wall-normal direction is examined in cases C1 and C2. Finally, the effect of not using the SGS model (unresolved DNS) is examined in cases A1 and A2.

The initial fields for the LES are for most cases obtained from a previous case, rather than from a laminar boundary-layer solution, to reduce the CPU cost in reaching the state of statistical equilibrium. Interpolation is performed when the grid is refined. In a few cases, the initial field was constructed after filtering a DNS flowfield from the simulation of Rai et al.[11] down to the grid used in the LES. The point of statistical equilibrium is determined by monitoring changes in the computed coefficient of skin friction. Statistical data are collected at every 10 time steps, until little change in the skin friction is observed with time. The mean fields are obtained after averaging in time and along the homogeneous, spanwise direction. All LES were run using a fixed time step, which was taken to be the same as the one used in the DNS, because the grid spacing used in the wall-normal direction for the LES was the same as that for the DNS.

B. Skin-Friction Coefficient

The skin-friction coefficient at the wall is defined in terms of the wall shear stress τ_w and freestream properties [$C_f = 2\tau_w/(\rho_\infty U_\infty^2)$]. Figures 2–4 show the variation of the computed coefficient of friction along the streamwise direction for the three sets of cases summarized in Table 1. The results are compared against the DNS data of Rai et al.,[11] the experimental data of Shutts et al.[15] (see Ref. 1), and the turbulent correlation of White and Christoff (see Ref. 16). As is shown in Fig. 2, the skin friction increases rapidly shortly after the location of blowing and suction as the flow is forced to transition to turbulence. The C_f from the turbulent correlation is about 10% higher than the reported experimental data of Shutts et al.[15] (see Ref. 1) and about 9% lower than the DNS data of Rai et al.[11] The overshoot seen in the DNS is typical of bypass transition. The results from case A2 (coarse grid DNS) are close to the correlation. However, as will be discussed in the following section, further evaluation of the results indicates that case A2 is underresolved. In evaluating the dynamic model, emphasis will be placed on the results from the DNS[11] for comparison. The most important finding from Fig. 2 is the fact that there seems to be a very small difference between the results from cases A1 and A2 in the turbulent region, indicating that the SGS model does not have a big effect on the accuracy of the LES, at least in predicting the correct skin friction.

The grid used for the LES of set B is twice as coarse in the spanwise direction compared with set A. As is shown in Figs. 3 and 4, lower values for the skin friction at the wall are predicted on the coarser grid. Although the dynamic model gave higher values of the eddy viscosity and eddy conductivity compared with set A, it is not able to make up the difference on accuracy of the computed C_f. (The comparison is again made with the DNS data.)

Different disturbance levels are used in cases B1 and B2. The disturbance amplitude $\mathcal{A}$ is gradually increased during the initial part of a simulation to avoid the sudden formation of pressure waves. As expected, the location of transition is moved farther upstream as $\mathcal{A}$ is increased (case B2). However, no difference on C_f is observed at $x = 8.8$ in., indicating that the flow there is fully turbulent. Therefore the differences seen in the LES when the grid is coarsened are not due to any end-stage (bypass) transition phenomena. This is supported also by a similar study, performed on an even coarser grid (see Fig. 4, cases C1 and C3).

Because the flow considered here is at relatively low turbulent Mach numbers, the modeling of the trace of the SGS stresses is not found to have a considerable effect on the computed C_f in the turbulent regime (cases B2 and B3).

Note that in temporal simulations[21,33,34] that use the dynamic model test filtering is usually not performed along the wall-normal direction. Test filtering in the y direction is performed in almost all of the spatially developing boundary-layer flow cases presented here. However, it is not found to have a big effect on the results, as can be seen in Fig. 4 for cases C1 and C2.

In addition, a version of the computer code was developed that uses third-order-accurate, upwind-biased differences for the convective terms and second-order central differences for the viscous terms. The effect of the numerical scheme is examined by comparing results from simulations that employed the (overall) second-order-accurate scheme to results from the (overall) fourth-order-accurate scheme. A significant drop in the computed skin-friction coefficient is found when the lower-order scheme is employed, as is shown in Figs. 3 and 4 for cases B1 and B4 and cases C1 and C4, respectively. These figures also show that the second-order scheme required about 2.65 times more grid points to match the results of the fourth-order scheme. The use of finite-difference-type schemes for spatial differencing does not allow for a good representation of the shorter resolved length scales.

Overall, the poor performance of the LES is believed to be due to the finite-difference errors (mainly damping errors) from the upwind scheme rather than the dynamic SGS model. These errors artificially damp the turbulence of the smaller resolved scales. Subgrid scales contain less energy than the grid scales. As a result, even accurate modeling of subgrid scales will not overcome the errors due to the finite difference scheme. Furthermore, because the dynamic model predicts the eddy viscosity and eddy conductivity based on the turbulence level of the smallest resolved scales, it provides insufficient amounts of turbulent transport. The observed effect of the finite difference errors on the LES results is consistent with the recent findings of Kravchenko and Moin,[35] who compared results from incompressible channel flow simulations using spectral and finite difference methods, and the earlier work of Beaudan and Moin,[30] who performed LES of incompressible flow past a cylinder using an upwind-biased finite difference scheme similar to the one that is also tested in this study.

Because the highly accurate spectral methods are not appropriate for use in complex flows, a possible solution to the problem would be to maintain only the information on the grid scales that are accurately resolved by a finite-difference-type scheme while modeling the effects of the scales that are omitted (including, of course, the subgrid scales). This approach, however, substantially increases the cost of the simulation because it requires explicit filtering of the contaminated modes at each time step using a high-order digital filter and the use of finer grids to ensure that the remaining resolved scales adequately represent the large eddies.[36,37]

Finally, the variation of the skin-friction coefficient with respect to the momentum thickness Reynolds number Re_θ is shown in Fig. 5 for several representative simulations. Also included are the C_f values from the experiments of Shutts et al.[15] (see Ref. 1) (reference case) and from the quasiequilibrium boundary-layer experiment of Elena and LaCharme,[17] which is at a slightly higher freestream Mach number and at a lower momentum thickness Reynolds number ($M = 2.32$ and $Re_\theta = 4.7 \times 10^3$). Compared with the latter experiment, the DNS overpredicts the skin friction, whereas all LES cases underpredict it. Furthermore, note that at the outlet plane of the turbulent region ($x = 9.0$ in.) the flowfields from the DNS and the LES are at a lower momentum thickness Reynolds number than the experimental value reported by Shutts et al.[15] (see Ref. 1) and therefore have different turbulence levels. This explains some of the differences seen in the results between the experiment and the simulations. In the LES, the reduced momentum thickness Reynolds number is due to the suppression of the turbulence due to finite difference errors. It is also clear that the SGS model cannot compensate for the numerical errors associated with the coarse grid.

C. Mean Velocity Profiles and Turbulence Statistics

This section includes a comparison of the mean velocity profiles as a function of the distance from the wall (in wall units), as well as the profiles of the resolved turbulence intensities, rms fluctuations, and turbulent shear stress at $x = 8.8$ in. for the flow cases of Table 1. Note that the DNS and experimental data here are not filtered to remove the scales not supported by the grids used in the LES, and some of the discrepancies may be due to SGS contributions to the turbulence quantities.

The variation of the Van Driest[38] velocity (normalized by the shear stress at the wall) with the normal distance from the wall at $x = 8.8$ in. is shown in Fig. 6 for cases A1, B1, and C1. Refining the grid again improved the agreement of the LES with the compressible law of the wall. Although the grid used in case A1 is only about a factor of three coarser than the DNS, there still seems to be room for improvement in accuracy. It appears that the effect of the numerical errors is to reduce the skin friction, which produces a log law that is too high, as shown in Fig. 6. Note, also, the excellent agreement between the DNS and the log law. However, the extended wake region found in the experimental data of Shutts et al.[15] (see Ref. 1) is not captured in the DNS. In addition, a smaller wake is seen in the data of Elena and LaCharme[17] because it is at a lower momentum thickness Reynolds number. Also, as is discussed (based on experimental findings) by Fernholtz and Finley,[39] exceptionally small wakes may be attributed to posttransitional effects. Therefore, it is possible that some remnants of the transition process are still present in the DNS at $x = 8.8$ in.

Figures 7–9 show the turbulence intensities normalized by the freestream velocity along the streamwise, wall-normal, and spanwise directions, respectively. As was mentioned earlier, turbulence fluctuation measurements were not taken by Shutts et al.[15] (see Ref. 1), and a wide variation in the value of the peak intensity is found in other existing compressible flow experimental data, especially when the measurements have been conducted using a

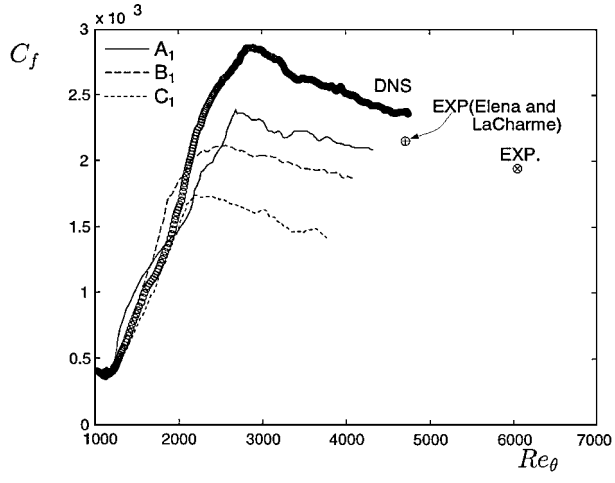

Fig. 5 Variation of skin-friction coefficient with Re_θ for several representative simulations.

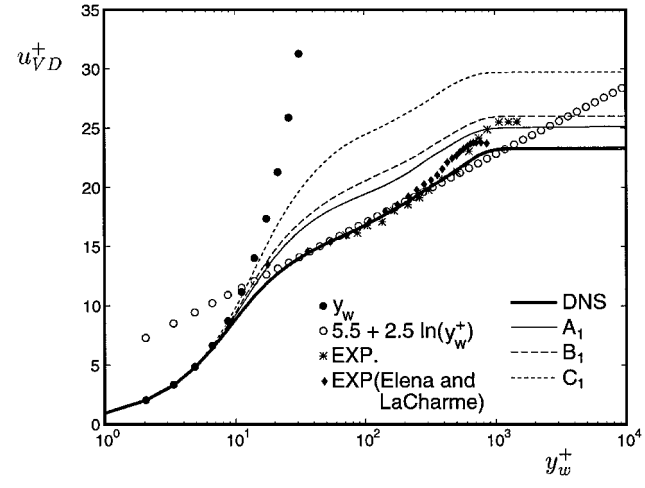

Fig. 6 Normalized Van Driest velocity profile at $x = 8.8$ in. for several representative simulations.

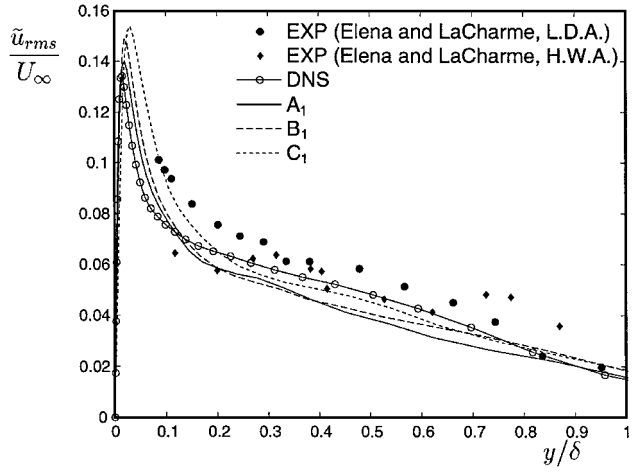

Fig. 7 Profiles of normalized, streamwise turbulent intensities at $x = 8.8$ in. for several representative simulations.

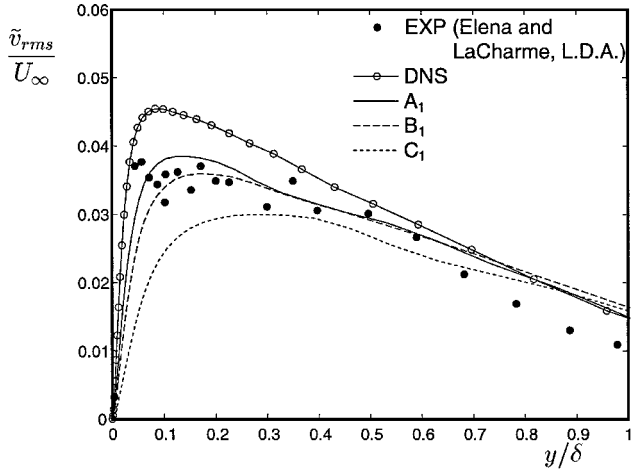

Fig. 8 Profiles of normalized, wall-normal turbulent intensities at $x = 8.8$ in. for several representative simulations.

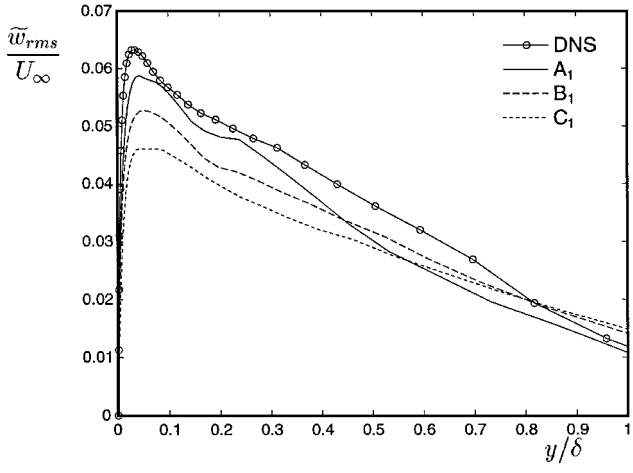

Fig. 9 Profiles of normalized, spanwise turbulent intensities at $x = 8.8$ in. for several representative simulations.

hot-wire anemometer (HWA).[17] Based on the study by Elena and LaCharme,[17] more accurate measurements can be obtained when a laser Doppler anemometer (LDA) is used instead. Also included in Figs. 7 and 8 for comparison are the turbulence intensity measurements from their recent experiment.[17] There are no available experimental data in the near-wall region, and so the LES results are compared quantitatively in this region only with the DNS data. The streamwise turbulence intensities for cases A1, B1, and C1 are shown in Fig. 7. Again, the agreement with DNS improves with grid refinement and with the use of a higher-order-accurate scheme. Otherwise, small differences are observed. The location and value of the peak intensity are overpredicted the most in set C because such grid resolution is too coarse to capture the important near-wall structures of the flow. The DNS data are lower than the LDA measurements and in better agreement with the HWA data. The DNS seems to overpredict the wall-normal, normalized intensities compared with the LDA measurements, as shown in Fig. 8. Much bigger differences, however, are seen in the predicted intensities between the LES and the DNS. Some of this discrepancy may be due to the fact that the DNS results have not been filtered and, therefore, include the SGS contribution. This issue is most significant for the wall-normal velocity component because it is more affected by the small scales. However, examination of one-dimensional spectra taken along the spanwise homogeneous direction reveals that, although the spectrum for the wall-normal velocity peaks at high wave numbers, the energy in the LES is suppressed for much of the high-wave-number-resolved scale range.[37] Therefore, the suppression observed is not simply due to the missing SGS contribution. The suppressed wall-normal velocities may be responsible for the reduced turbulent transport of momentum and thereby the reduced skin friction observed in the preceding section. Similar trends are observed in the profiles of the spanwise turbulent intensities in Fig. 9.

The turbulent intensities normalized by the local mean streamwise velocity are plotted in wall units at $x = 8.8$ in. in Figs. 10–12. Because compressibility effects in this flow are not strong and because experimental data close to the wall are not available for this kind of flow, the data from an incompressible flow flat-plate experiment[40] are included for comparison. The results are mixed here. Good agreement is found between the DNS and case A1 in Fig. 10. All

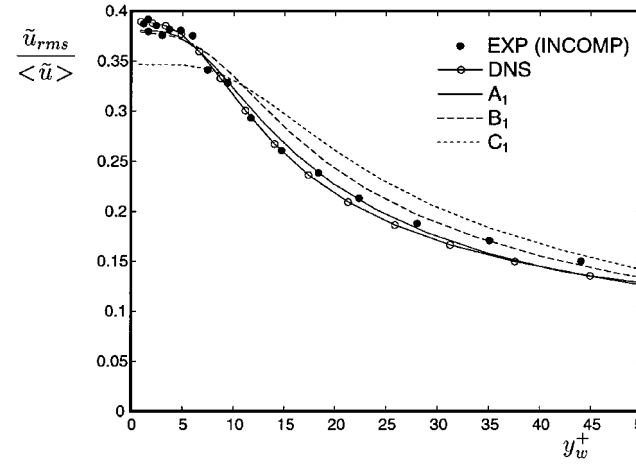

Fig. 10 Profiles of normalized, streamwise turbulent intensities in wall coordinates at $x = 8.8$ in. for several representative simulations.

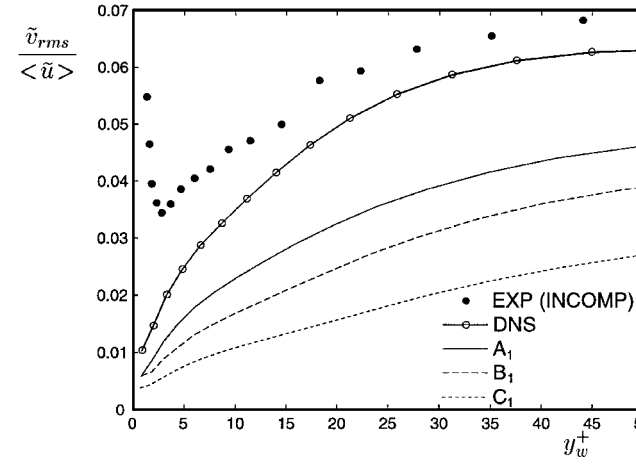

Fig. 11 Profiles of normalized, wall-normal turbulent intensities in wall coordinates at $x = 8.8$ in. for several representative simulations.

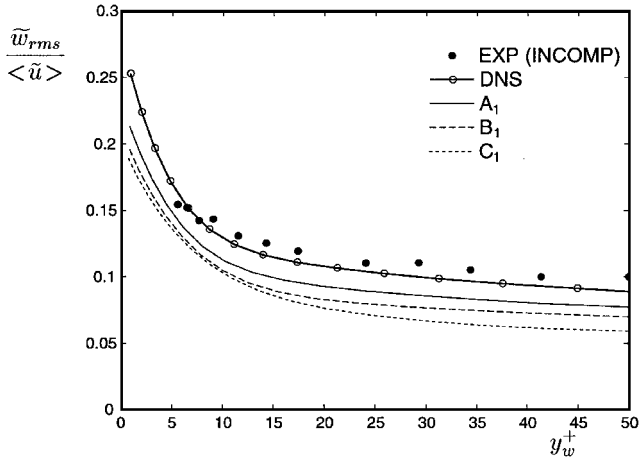

Fig. 12 Profiles of normalized, spanwise turbulent intensities in wall coordinates at $x = 8.8$ in. for several representative simulations.

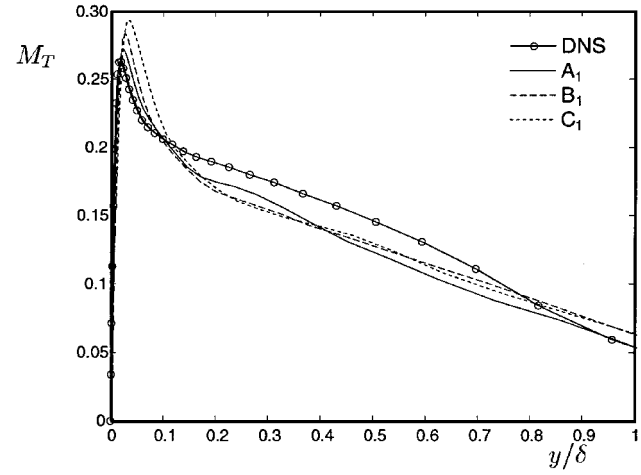

Fig. 13 Profiles of turbulent Mach number at $x = 8.8$ in. for several representative simulations.

cases underpredict the wall-normal intensities, as is shown in Fig. 11. However, better agreement is seen for the spanwise intensities. The discrepancy in the results is the largest in C1. The streamwise and spanwise turbulence intensities from the DNS data are close to the experimental data, whereas a suppression of the wall-normal intensities is observed in the simulations. In the region close to the wall, however, the experimental data for the wall-normal intensities unphysically increase and are in error. The data should instead vanish linearly with y, as can be shown easily from a Taylor series analysis, with the aid of the continuity equation. Note that the profiles of the turbulence intensities at several upstream distances close to $x = 8.8$ in. were also examined and found to be almost identical, indicating that the outflow boundary condition is not significantly affecting the results.

The distribution of the turbulent Mach number, $M_T = \sqrt{[\bar{\rho}\widetilde{u_i''u_i''}/(\gamma\bar{p})]}$, is shown in Fig. 13. The maximum value of M_T is less than 0.3, in support of the previously made argument that the turbulent flow considered here is not strongly compressible.

Figure 14 shows the Reynolds shear stress profile at $x = 8.8$ in. in wall units (normalized by the square of the wall shear velocity). Good agreement for case A1 is seen near the wall region. However, the results deteriorate in B1 and, even more, in C1.

Shown in Fig. 15 are the computed one-dimensional spectra of the spanwise velocity component taken along the spanwise homogeneous direction at $x = 8.8$ in. and $y = 0.00274$ in. for the DNS and cases A1, B1, and C1. As the grid is refined, the results tend toward the DNS data. The LES on coarser grids is very dissipative, especially at the smaller resolved scales.

Finally, a contour plot of the time and spanwise averaged ratio μ_t/μ is shown for case B1 in Fig. 16. In this case, the eddy viscosity

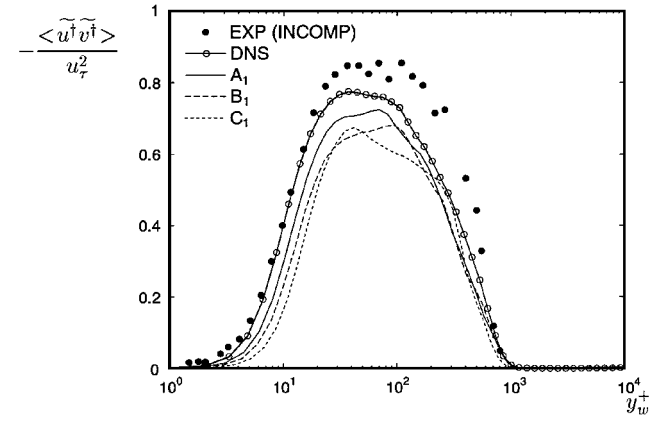

Fig. 14 Normalized, resolved Reynolds shear stress in wall coordinates at $x = 8.8$ in. for several representative simulations.

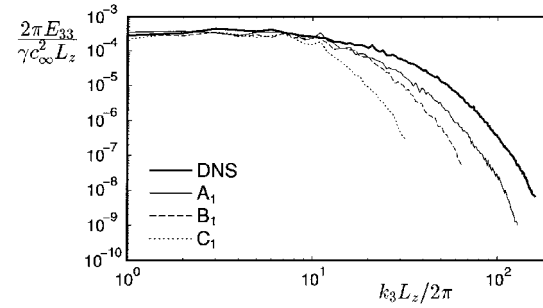

Fig. 15 Spanwise one-dimensional spectra of the spanwise velocity component at $x = 8.8$ in. and $y = 0.00274$ in. for several representative simulations.

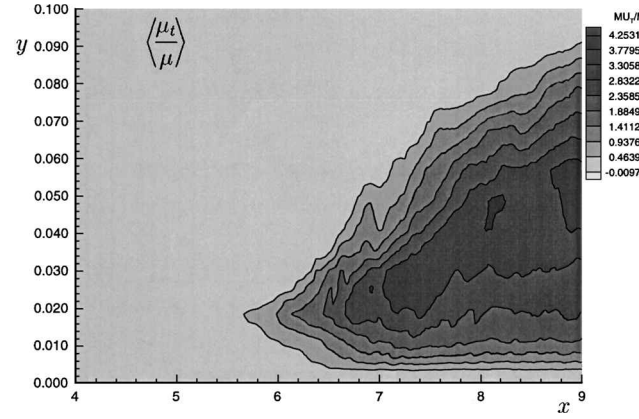

Fig. 16 Spanwise and time-averaged ratio of eddy to molecular viscosity for case B1.

is at most 4.3 times greater than the molecular viscosity. (Similar findings were seen for k_t/k.) Inside the boundary layer, the dynamic model is found to vanish in the near-wall region and toward the edge of the boundary layer, as well as in the laminar regime (the model is turned off outside the boundary layer). Also, when the grid was refined or coarsened, the model gave lower or higher values, respectively, for these ratios, as expected. The isotropic part, $\frac{1}{3}\tau_{kk}$, of the SGS stress tensor for this flow is predicted by the model to be at most 8% of the thermodynamic pressure $\bar{p}$ and could be neglected. Finally, the variation of the dynamic model coefficient C was similar to that of μ_t/μ.

VII. Conclusions

A number of issues involved in the LES of spatially evolving supersonic boundary layers are examined by conducting simulations using a high-order-accurate finite difference scheme and the dynamic SGS model. The computational grid was refined successively to improve the agreement of the computed turbulence statistics with

the available experimental data and results from a DNS calculation. The grids used in the LES are from 16 up to 3 times coarser than the grid used in the DNS. The computational domain is found to be long enough for the flow to reach a fully turbulent state free of transients due to the periodic blowing and suction mechanism employed to bypass the natural transition process.

The results suggest that the finite difference scheme has a direct effect on the dynamic SGS model, reducing greatly the accuracy of the simulations. Numerical errors from the finite difference method can be large enough that the SGS model has little effect on the solution. The use of a higher-order scheme is found to improve substantially the results because it improves the capture of the smaller resolved scales. Furthermore, it is recommended to apply the model not only at the subgrid scales but also at the scales that are not properly resolved by the numerical scheme. This approach, however, will substantially increase the cost of the simulation, in terms of both CPU time and memory requirements, because it requires explicit grid filtering (using a highly accurate filter) of the flowfields at each time step and the use of finer grids. The effect of descretization errors on LES needs to be addressed further before proceeding with LES of flows of engineering interest.

Acknowledgments

This work was supported in part by NASA Langley Research Center under Grant NAG-1-1509. Computer resources were provided by the Numerical Aerodynamic Simulation facility. The authors are indebted to the Technical Monitor, Thomas Gatski, for his valuable insight and suggestions. The many helpful conversations with Man M. Rai, Ugo Piomelli, John Cimbala, and Joseph Morrison are also appreciated.

References

[1]Fernholz, H. H., and Finley, P. J., "A Critical Compilation of Compressible Turbulent Boundary Layer Data," AGARDograph 223, June 1977 (Case 55010501).

[2]Fernholz, H. H., and Finley, P. J., "A Further Compilation of Compressible Turbulent Boundary Layer Data with a Survey of Turbulence Data," AGARDograph 263, Nov. 1981.

[3]Fernholz, H. H., Smits, A. J., Dussauge, J. P., and Finley, P. J., "A Survey of Measurements and Measuring Techniques in Rapidly Distorted Compressible Turbulent Boundary Layers," AGARDograph 315, May 1989.

[4]Settles, G. S., and Johnson, L. J., "Hypersonic Shock-Boundary Layer Interaction Database," NASA CR-177577, 1991.

[5]Spina, E. F., Smits, A. J., and Robinson, S. K., "The Physics of Supersonic Turbulent Boundary Layers," *Annual Review of Fluid Mechanics*, Vol. 26, 1994, pp. 287–319.

[6]Bradshaw, P., "Compressible Turbulent Shear Layers," *Annual Review of Fluid Mechanics*, Vol. 9, 1977, pp. 33–54.

[7]Lele, S. K., "Compressibility Effects on Turbulence," *Annual Review of Fluid Mechanics*, Vol. 26, 1994, pp. 211–254.

[8]Smits, A. J., and Dussauge, J. P., "Hot-Wire Anemometry in Supersonic Flow," AGARDograph 315, May 1989, Chap. 5.

[9]Kistler, A. L., "Fluctuation Measurements in a Supersonic Turbulent Boundary Layer Flow," *Physics of Fluids A*, Vol. 2, May–June 1959, pp. 290–296.

[10]Spina, E. F., Donovan, J. F., and Smits, A. J., "On the Structure of High-Reynolds-Number Supersonic Turbulent Boundary Layers," *Journal of Fluid Mechanics*, Vol. 222, Jan. 1991, pp. 293–327.

[11]Rai, M. M., Gatski, T. B., and Erlebacher, G., "Direct Simulation of Spatially Evolving Compressible Turbulent Boundary Layers," AIAA Paper 95-0583, Jan. 1995.

[12]Childs, R. E., and Reisenthel, P. H., "Simulation Study of Compressible Turbulent Boundary Layers," AIAA Paper 95-0582, Jan. 1995.

[13]Hatay, F. F., and Biringen, S., "Direct Numerical Simulation of Low-Reynolds-Number Supersonic Turbulent Boundary Layers," AIAA Paper 95-0581, Jan. 1995.

[14]Guo, Y., and Adams, N. A., *Proceedings of the 1994 Summer Program*, NASA/Stanford Center for Turbulence Research, Stanford, CA, 1994, pp. 245–267.

[15]Shutts, W. H., Hartwig, W. H., and Weiler, J. E., "Final Report on Turbulent Boundary Layer and Skin Friction Measurements on a Smooth, Thermally Insulated Flat Plate at Supersonic Speeds," Deutsche Forschungsanstalt für Luft- und Raumfahrt, Rept. 364, 1955.

[16]White, F. M., *Viscous Fluid Flow*, McGraw–Hill, New York, 1991, pp. 552–554.

[17]Elena, M., and LaCharme, J. P., "Experimental Study of a Supersonic Turbulent Boundary Layer Using a Laser Doppler Anemometer," *Journal de Mécanique Théorique et Appliquée*, Vol. 7, No. 2, 1988, pp. 175–190.

[18]Erlebacher, G., Hussaini, M. Y., Speziale, C. G., and Zang, T. A., "Toward the Large-Eddy Simulation of Compressible Turbulent Flows," *Journal of Fluid Mechanics*, Vol. 238, May 1992, pp. 155–185.

[19]Moin, P., Squires, K., Cabot, W., and Lee, S., "A Dynamic Subgrid-Scale Model for Compressible Turbulence and Scalar Transport," *Physics of Fluids A*, Vol. 3, Nov. 1991, pp. 2746–2757.

[20]Huang, P. G., Coleman, G. N., and Bradshaw, P., "Compressible Turbulent Channel Flows: DNS Results and Modeling," *Journal of Fluid Mechanics*, Vol. 305, Dec. 1995, pp. 185–218.

[21]Germano, M., Piomelli, U., Moin, P., and Cabot, W., "A Dynamic Subgrid-Scale Eddy-Viscosity Model," *Physics of Fluids A*, Vol. 3, July 1991, pp. 1760–1765.

[22]Lilly, D. K., "A Proposed Modification of the Germano Subgrid-Scale Closure Method," *Physics of Fluids A*, Vol. 4, March 1992, pp. 633–635.

[23]Wong, V. C., "A Proposed Statistical-Dynamic Closure Method for the Linear or Nonlinear Subgrid-Scale Stresses," *Physics of Fluids A*, Vol. 5, May 1992, pp. 1080–1082.

[24]Ghosal, S., Lund, T. S., and Moin, P., "A Local Dynamic Model for Large-Eddy Simulation," *Annual Research Briefs—1992*, Center for Turbulence Research, Stanford Univ., Stanford, CA, Dec. 1992, pp. 3–25.

[25]Piomelli, U., and Liu, J., "Large-Eddy Simulations of Rotating Channel Flows Using a Localized Dynamic Model," *Physics of Fluids A*, Vol. 7, April 1995, pp. 839–848.

[26]Smagorinsky, J. S., "General Circulation Experiments with the Primitive Equations. I. The Basic Experiment," *Monthly Weather Review*, Vol. 91, March 1963, pp. 99–164.

[27]Yoshizawa, A., "Statistical Theory for Compressible Turbulent Shear Flows, with the Application to Subgrid Modeling," *Physics of Fluids A*, Vol. 29, July 1986, pp. 2152–2164.

[28]Chakravarthy, S. R., Anderson, D. A., and Salas, M. D., "The Split-Coefficient Matrix Method for Hyperbolic Systems of Gas Dynamic Equations," AIAA Paper 80-0268, Jan. 1980.

[29]Rai, M. M., and Moin, P., "Direct Numerical Simulation of Transition and Turbulence in a Spatially Evolving Boundary Layer," *Journal of Computational Physics*, Vol. 109, Dec. 1993, pp. 169–192.

[30]Beaudan, P., and Moin, P., "Numerical Experiments on the Flow Past a Circular Cylinder at Sub-Critical Reynolds Number," Dept. of Mechanical Engineering, Stanford Univ., Rept. TF-62, Stanford, CA, Dec. 1994.

[31]Konzelmann, U., Rist, U., and Fassel, H., "Erzeugung Dreidimensionaler, Räumlich Angefachter Störwellen Durch Periodisches Ausblasen und Absaugen in Einer Plattengrenzschichtströmung," *Zeitschrift für Angewandte Mathematik und Mechanik*, Vol. 67, No. 5, 1987, pp. T298–T300.

[32]Rist, U., and Fasel, H., "Direct Numerical Simulation of Controlled Transition in a Flat-Plate Boundary Layer," *Journal of Fluid Mechanics*, Vol. 298, Sept. 1995, pp. 211–248.

[33]Piomelli, U., "High Reynolds Number Calculations Using the Dynamic Subgrid-Scale Model," *Physics of Fluids A*, Vol. 5, June 1993, pp. 1484–1490.

[34]Akselvoll, K., and Moin, P., "Large-Eddy Simulation of Turbulent Confined Coannular Jets and Turbulent Flow over a Backward Facing Step," Dept. of Mechanical Engineering, Stanford Univ., Rept. TF-63, Stanford, CA, Feb. 1995.

[35]Kravchenko, A. G., and Moin, P., "On the Effect of Numerical Errors in Large-Eddy Simulations of Turbulent Flows," *Journal of Computational Physics*, Vol. 131, March 1997, pp. 310–322.

[36]Lund, T. S., and Kaltenbach, H.-J., "Experiments with Explicit Filtering for LES Using a Finite Difference Method," *Annual Research Briefs—1995*, Center for Turbulence Research, Stanford Univ., Stanford, CA, Dec. 1995, pp. 91–105.

[37]Spyropoulos, E., "On Dynamic Subgrid-Scale Modeling for Large-Eddy Simulation of Compressible Turbulent Flows," Ph.D. Thesis, School of Aeronautics and Astronautics, Purdue Univ., West Lafayette, IN, Dec. 1996.

[38]Van Driest, E. R., "On the Turbulent Flow near a Wall," *Journal of the Aeronautical Sciences*, Vol. 23, Nov. 1956, pp. 1007–1011.

[39]Fernholz, H. H., and Finley, P. J., "A Critical Compilation of Compressible Turbulent Boundary Layer Data," AGARDograph 223, June 1977 (Catalog Entry 5802).

[40]Karlson, R. I., and Johansson, T. G., "LDV Measurements of Higher-Order Moments of Velocity Fluctuations in a Turbulent Boundary Layer," *Laser Anemometry in Fluid Mechanics*, Ladoan-Instituto Superior Tecnico, Lisbon, Portugal, 1988.

C. G. Speziale
Associate Editor